PROCEEDINGS, 41st Workshop on Geothermal Reservoir Engineering
Stanford University, Stanford, California, February 22-24, 2016
SGP-TR-209

Laboratory Scale Investigation of Enhanced Geothermal Reservoir Stimulation

Lianbo Hu, Ahmad Ghassemi

The University of Oklahoma, Norman, OK 73019 USA

ahmad.ghassemi@ou.edu

John Pritchett, Sabodh Garg

Leidos Inc.

Keywords: Enhanced geothermal systems, stimulation, acoustic emission, spontaneous potential

ABSTRACT

Geothermal energy production by water circulation in natural and/or man-made fracture systems is referred to as enhanced or engineered geothermal systems (EGS). The permeable zones of an EGS must be created by stimulation, a process which involves fracture initiation and/or activation and propagation of discontinuities such as joints by pore pressure and stress perturbations. Economic design and operation of EGS can be achieved by reliable characterization of the stimulation results which relies mostly on analysis of MEQ and tracers. In this work we study the reservoir stimulation process on a laboratory scale to improve the current understanding and to help quantify the fracture geometry using acoustic emission (AE) cloud, spontaneous potential (SP), and tracer analysis. To do so, we have developed a new poly-axial hydraulic fracturing test system which allows us to perform reservoir stimulation experiments on rock blocks with size up to 18' x18" x 18" under high pore pressure and representative in-situ stress regimes while simultaneously recording SP and AE during fracturing and circulation. The system can operate at relatively high temperatures (150^{o}C). In this paper, we describe preliminary experiments conducted at room temperature. Results show excellent correlation between fracturing and the SP signal. Also, stimulation has been accompanied by AE events that are generally correlated with the stress state and fracture geometry.

1. INTRODUCTION

Geothermal energy is considered as a promising option for future clean and sustainable energy supply (MIT-led Report, 2006). However, certain technical barriers need to be removed for large scale utilization of the resources. Particularly, questions related to reservoir creation in different rock types and stress conditions need be addressed. Laboratory scale studies present a good opportunity to help resolve some of the pending challenges along with recent field-scale efforts within the framework of the FORGE initiative. The main purpose of this project is to gain a better understanding of the geometry and the heat exchange properties of the hydraulically induced fractures in EGS. To realize this goal, a new lab-scale hydraulic fracture test system has been developed that allows us to replicate aspects of the EGS hydraulic fracturing treatment in the field. Our work improves the state-of-the-art by allowing the simultaneous monitoring of AE, SP and tracers during the stimulation and circulation phases.

2. THE LAB-SCALE EGS TEST SYSTEM

The lab-scale EGS system has several integrated subsystems. The main subsystems are: a polyaxial frame and heaters, hydraulic fracturing and circulation system, AE and SP acquisition system, and fluids and tracers. The core of the newly developed system is the polyaxial frame which has the capacity to accept and load a cubical rock sample with three independently controlled total principal stresses up to 5000 psi. The loading frame can be sealed with high pore pressure in the rock (around 1500 psi). Sensors are used on the block surfaces and within cavities to characterize and locate acoustic emissions caused by the stimulation, and to monitor local changes in fluid pressure, temperature and spontaneous potential (also known as self-potential). Cold water containing a tracer can be injected and simultaneously collected from nearby miniature production wells. Relevant data are collected and analyzed to develop a better understanding of the fractures and the induced fracture permeability and fluid/heat flow. The system allows for multiple injection/production wells. Currently, we are using one injection well located in the center of the block and four surrounding production wells for continuous water circulation to help characterize the fluid/heat flow process.

Figure 1 (left) shows the partially assembled polyaxial frame, which consists of three parts: the bottom and top lids and the cylindrical housing. In the picture, we can see the top lid, cylindrical housing, the bottom lid, the insulation foam (red) and the Faraday cage jacket. The fully assembled frame is shown in Figure 1 (right). The principal stresses are applied to the sample using three flatjacks. A polyaxial frame or true triaxial frame is not new in hydraulic fracturing experimentation, but this polyaxial frame is capable of handling fluid pressure while allowing signal wires and hydraulic lines to pass out of the frame without leakage. This feature allows us to simulate hydraulic fracturing tests on saturated samples with controllable pore pressure.

For sample heating, we developed a hot water circulation system. After the polyaxial frame is assembled with a rock sample inside, the desired saturation fluid is poured into the frame and water circulation starts. The heater in the circulation system heats the rock efficiently, since the water has a large contact area with the rock. Also the silicone rubber heaters on the sides and bottom of the frame will help accelerate this process. Once the temperature of the rock sample reaches the desired temperature, which is determined by temperature sensors on/ in the rock sample, the circulation is stopped and the tubing connected to the frame is closed, and then a silicone

rubber heater with a PID controller helps maintain constant temperature at the boundaries of the rock block. As shown in Figure 2, the pump, water tank and heater are assembled on a small car. The insulation foam on the surface of the frame helps minimize the heat loss from the frame and a Faraday cage jacket is present to block electric fields from the outside of the frame.

Figure 1: Polyaxial frame with insulation foam (red) and the Faraday cage jacket (black).

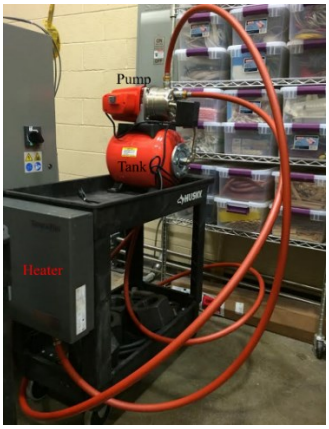

Figure 2: Hot water circulation system.

Figure 3 (left) is a top view showing the layout of the wells and the AE sensors on the top surface, and Figure 3 (right) is a longitudinal sectional view of the sample showing the interior layout of the wells. The injection hole was drilled using a 0.75 inch diameter drill bit. The drilled injection well has a depth of 7.5 inches and a diameter of 0.78 inch. High strength epoxy is poured into the hole to seal the annulus between the injection tubing and the wellbore wall leaving a 2 inch unsealed injection interval at the bottom. Four production wells with a depth of 9 inch are drilled 3.5 inches away from the injection well and have 5 inch unsealed production intervals at the bottom. The diameter of the production wells is 0.4 inch. An SP sensor is placed in the injection well as a reference electrode. The SP sensors were made by soldering a coaxial cable to a thin circular copper sheet with a diameter of 0.5 inch. Small alundum (aluminum oxide) balls are located inside the production wells to occupy space in an effort to minimize the effect of wellbore storage.

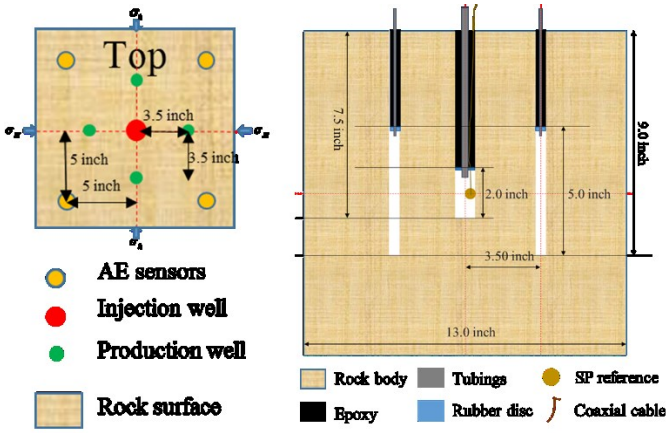

Figure 3: Layout of injection well and production wells with sensors.

The injection of fluids is carried out using a Teledyne Isco syringe pump with an injection rate less than 5 ml/min. To control the injection process and thus hydraulic fracture propagation, a LABVIEW program has been developed to control the injection process. Through the program we can control the injection rate and injection conditions (constant pressure or constant flowrate). Once a pre-determined pressure drop is detected, the injection rate is reduced by 99 percent to attempt to prevent uncontrolled fracture propagation.

After the fracturing process, cold water with tracers is injected into the injection well and fluid produced from the production wells is collected for chemical analysis. The fluid temperature at the injection interval and production intervals is recorded. In order to control the production pressure in the production wells and also to collect production fluid continuously, a production control system is used as shown in Figure 4. The pressure transducer can measure the pressure in the production well; the filter will keep the adjustable relief valves from being damaged by solid particles coming out with the production fluid. The adjustable relief valve is used to control the production pressure.

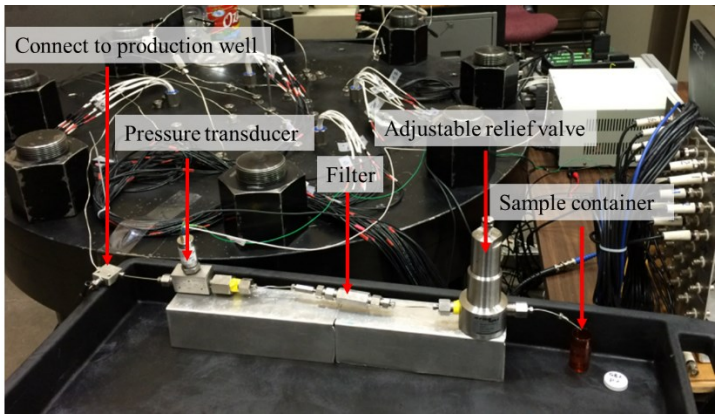

Figure 4: Production control system.

The SP response during the hydraulic fracturing treatment is detected by the SP sensors on the surface of the rock sample and recorded by a data logger with an impedance of 20 GΩ and maximum scan rate of 100 kHz. High data logger impedance was selected to minimize instrument loading (Moore and Glaser, 2007). The SP sensors were made by soldering a coaxial cable to a thin circular copper sheet with a diameter of 0.5 inch. For our preliminary test, the SP sensors were attached to only one surface of the rock, but for our future tests SP sensors will be placed on four or five surfaces of the rock to help determine the fracture geometry. Six nonconductive PEEK plastic plates are placed on the rock sample surface to electrically isolate the rock from the steel spacers and flatjacks. Grooves and cavities on the PEEK plates provide housing for the SP and AE sensors.

To detect the Acoustic Emission signals during the fracture initiation and propagation, sixteen PZT-5A piezoelectric transducers with a resonance frequency of 500 kHz are located on the rock surfaces. The signals received are amplified by a MISTRAS 2/4/6 preamplifier with 40 dB gain to increase the signal to noise ratio (Yang, 2012). The amplified signal is recorded and analyzed by a MISTRAS Express-8 AE system, which allows us to determine the location and failure mode of each AE event.

Before we tested cubical rock blocks, water solutions with different inorganic salts were used as saturation fluid and injection fluid on small cylindrical samples for SP detection during hydraulic fracturing. The concentration of the salts were around 0.002 mol/L and good SP signals were obtained during these tests. For block tests, the injection fluid is the same as the solution that saturates the rock block. For the test discussed below a 1:1 mixture of 0.002 mol/L Sodium Chloride (NaCl) and 0.002 mol/L Sodium Bromide (NaBr) was used as the tracer during the circulation test. But, considering the high cost for post concentration measurement of the production fluid, organic tracer such as Butanol could be added as tracer.

3. PRELIMINARY TEST RESULTS

3.1 Test Setup

A 13 inch cubical Sierra White granite block was instrumented with AE and SP sensors and placed in the frame to verify the proposed test methodology and expose as many potential issues as possible. The well layout is the same as that shown in Figure 3 and the locations of SP sensors and AE sensors are shown in Figure 5. Four small piezoelectric transducers were also placed at the bottom of the production wells. Then, the sample was saturated and the principal stresses were applied by injecting high pressure fluid into the flatjacks. The space between the rock sample and inner surface of the cylindrical housing is occupied by flatjacks, PEEK plates and steel plate spacers. We conducted two cycles of fracturing-circulation test on the rock block. The test conditions and result are discussed below.

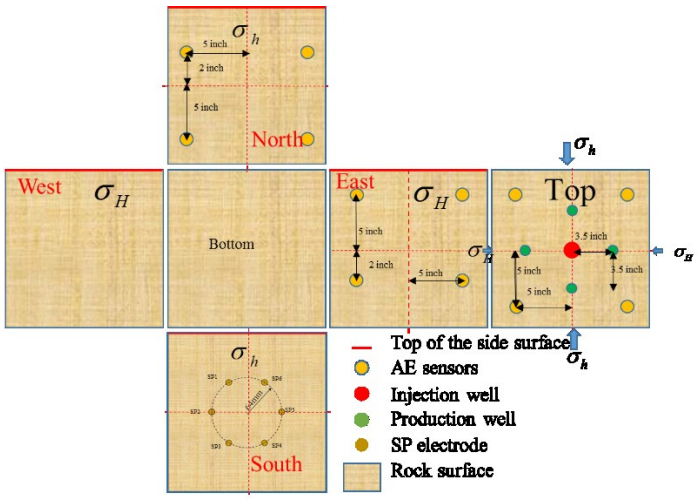

Figure 5: Fold-out diagram of the Sierra White block with AE sensors and SP sensors.

3.2 Test Parameters and Results of the First Cycle of Fracturing-Circulation Test

Before the test, the rock sample was saturated with 0.002mol/L Calcium nitrate ($Ca(NO_3)_2$) solution. The same solution was used for fracturing. The stress conditions for this test are listed in Table 1. After the fracturing, a 1:1 mixture of 0.002 mol/L NaCl and 0.002 mol/L NaBr was used as the tracer fluid.

Table 1: Experimental parameters for Sierra White granite block (first cycle)

p_p, psi	σ_V, psi	σ_h, psi	σ_H, psi
200	550	380	450

Figure 6 shows the recorded data for the test, namely injection pressure (red), flow rate (green), SP response (black, SP1), accumulation of AE events (blue) and the injection volume (purple). The injection rate was set to be 2 ml/min to have better control of the propagation of the fracture. The controlling program reduced the injection rate to 0.02 ml/min right after the pressure drop exceeded the preset value (the first inflection point on the pressure plot). Twenty seconds later, the injection rate was reset to the initial value and this second injection stage lasted 66 s. Then, pumping ceased. From the test result, it is clear that the injection pressure and the SP response are in proportion to each other. Also, it can be seen that the proportionality factor between SP and pressure is different before and after fracturing. The SP-pressure drop response indicates that electrokinetic mechanism was the main source for the SP and also the newly-created microcracks and fractures decreased the hydraulic tortuosity and increased the permeability of the related zones. The zeta potential of the new fracture surface area also may be higher than that of the rock body and thereby contribute to the higher proportionality factor.

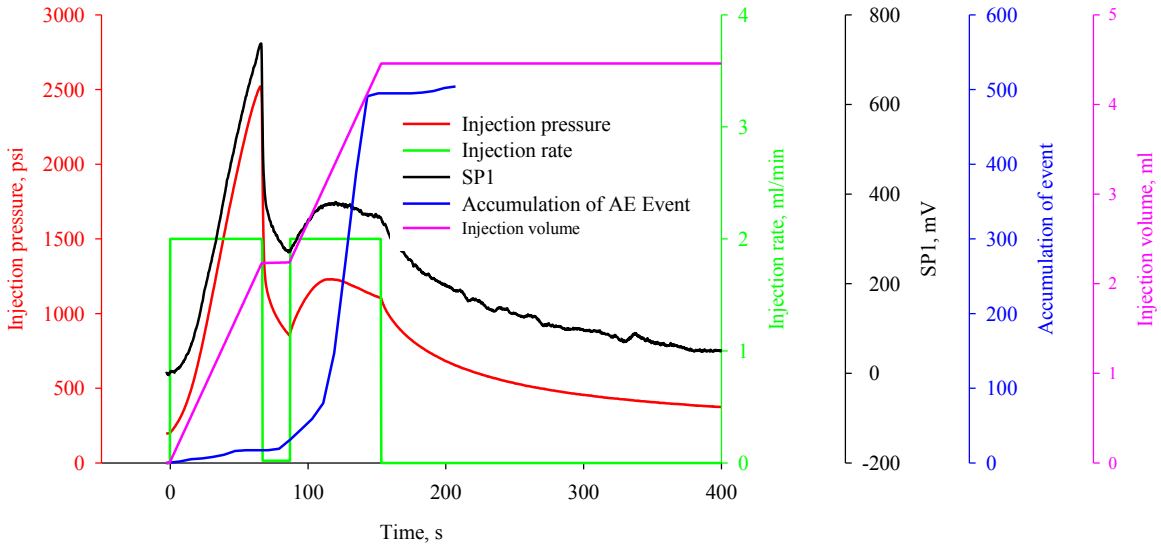

Figure 6: The recording data for Sierra White granite block test (first cycle).

The cumulative AE event count indicates that most of the fracturing took place during the second stage of injection. The breakdown pressure was 2520 psi which is 42% higher than the theoretical value calculated from Hubbert and Willis model (Equation 1):

$$p_b = 3\sigma_h - \sigma_H - p_p + \mathrm{T} \tag{1}$$

where p_b, p_p, σ_h, σ_H, T are breakdown pressure, pore pressure, minimum horizontal principal stress, maximum horizontal principal stress and tensile strength of the rock, respectively. The wellbore size effect and the rock heterogeneity could be the main reasons for this phenomenon. A vertical wellbore geometry is assumed in this equation. The tensile strength of Sierra White granite was measured to be 1280 psi from the Brazilian test. The fracture propagation pressure is around 850 psi based on the instantaneous shut-in pressure, which is much higher than the minimum horizontal stress. But considering that the induced fracture was still near the wellbore and that it had two parts, the difference can be understood.

To provide a better understanding of the relationship between the pressure drop (pressure difference between the location of the reference sensor-injection well- and the SP signal sensor), and the SP recording (the potential difference between the SP sensors on the rock surface and the SP reference electrode in the injection well) the pressure drop vs SP is plotted in Figure.7, which shows excellent proportionality between pressure drop and SP response. The time interval is divided into two subintervals: before and after fracturing. The electrokinetic coupling coefficient is defined as the ratio of SP to pressure difference shown in Equation (2) (Jouniaux and Pozzi , 1995). For the interval before fracture, the electrokinetic coupling coefficient has a value is 0.3029 mV/psi and its value is 0.3772mV/psi after fracturing (Figure 8). After fracturing, the coefficient increased about 25%. This increase of electrokinetic coupling coefficient is caused by the increased permeability at higher pore pressure due to dilatancy of microcracks and the related decreased hydraulic tortuosity and the possible increase of zeta potential of new fracture surface area also could contribute to the higher proportionality factor.(Moore and Glaser, 2007):

$$Cc = \frac{\Delta\varphi}{\Delta p} = \frac{\varepsilon\zeta}{\eta\sigma_f}\frac{F}{F_o} \tag{2}$$

where Cc, φ, p, ε, ζ, η, σ_f, F, and F_o are electrokinetic coupling coefficient, electric potential, fluid pressure, absolute dielectric constant of the fluid, zeta potential, dynamic fluid viscosity, fluid conductivity, formation factor for the current sample conditions, and electrical formation factor respectively. Equation (2) is based on the assumption that the fluid flow is laminar, which requires low injection rate during the injection (Fitterman, 1978; Morgan, 1989).

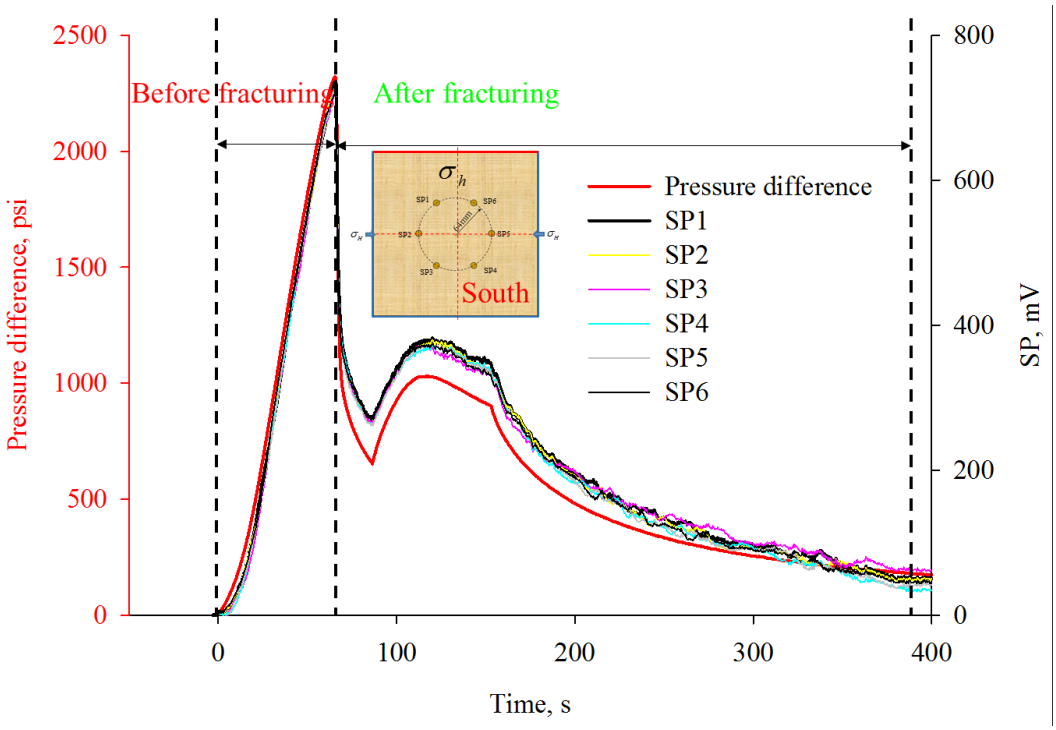

Figure 7: The SP data with pressure drop (first cycle).

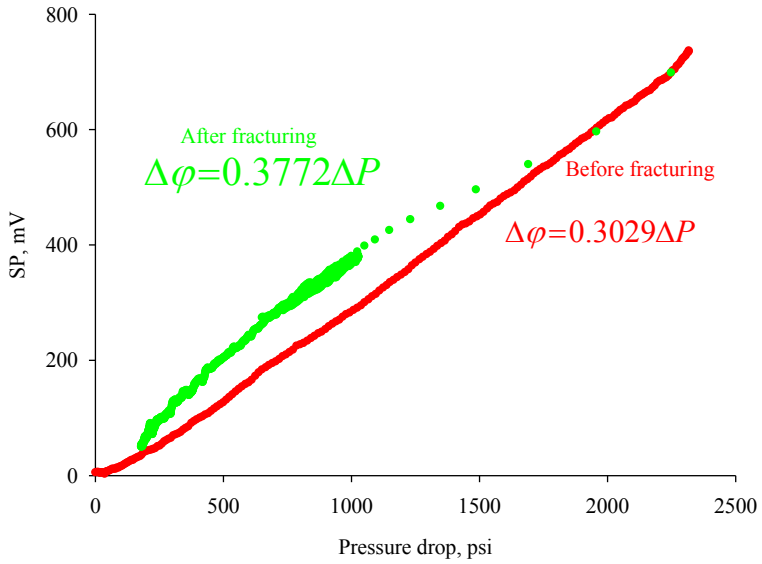

Figure 8: The electrokinetic coupling coefficient for different intervals (first cycle).

3.3 Test Parameters and Result of the Second Fracturing-Circulation Test Cycle

After the first fracturing-circulation cycle, a re-fracture and circulation test was conducted. The purpose of this test was to generate a horizontal fracture which would have a better chance of intersecting the production wells since the initial fracturing attempt did not intersect any of the production wells. From the result of post-test analysis, this goal was successfully achieved. The original minimum horizontal stress was changed to 1200 psi and the original maximum horizontal stress was changed to 700 psi while the vertical stress was maintained as 550 psi. Table 2 lists the stress condition for the second test. During the second test, AE information was not recorded due to inadvertent AE system shut-down. In this test, the injection and circulation fluid was a 1:1 mixture of 0.002 mol/L NaCl and 0.002 mol/L NaBr. Figure 9 shows the result of the second test including the injection pressure, SP response, and the flowrate and injection volume. A very good relationship between the SP and pressure difference can be observed.

Table 2: Experimental parameters for Sierra White granite block (second cycle)

P_p , psi	σ_V , psi	σ_h , psi	σ_H , psi
200	550	700	1200

The second test is divided into four subintervals according to the injection process namely, Injection-1, Injection-2, Shut-in and Circulation. At t_1=172s, the injection pressure drops dramatically at a constant injection rate, which indicates that the induced fracture intersected a production well(s). After the test, the rock block was cut into two pieces, revealing the intersection of the fracture and one of the production wells. For both the Injection-1 and Injection-2 intervals, the peak pressure is about 830 psi, which corresponds to the re-frac stress state with a vertical stress of 550 psi.

Figure 10 shows the SP responses recorded by all six SP sensors. It is clear that during the initial part of the test, the SP response is related linearly to the pressure drop. But beyond t_2=250s, this relationship becomes weak and also the SP responses recorded by the various SP sensors start diverging. This indicates that the fracture has reached the outer surface of the rock block at time t_2.= 250-300s. As before, a plot showing the pressure drop and SP response is provided in Figure 11. Only the data before t_2=250s are considered since the SP response after the fracture reaches the rock block boundary is less predictable (Moore and Glaser, 2007). The electrokinetic coupling coefficient is determined as about 0.6mV/psi, which is much higher than that from the first fracturing cycle test. This is probably due to the changing of the injection fluid and the increased permeability of the fracture zone.

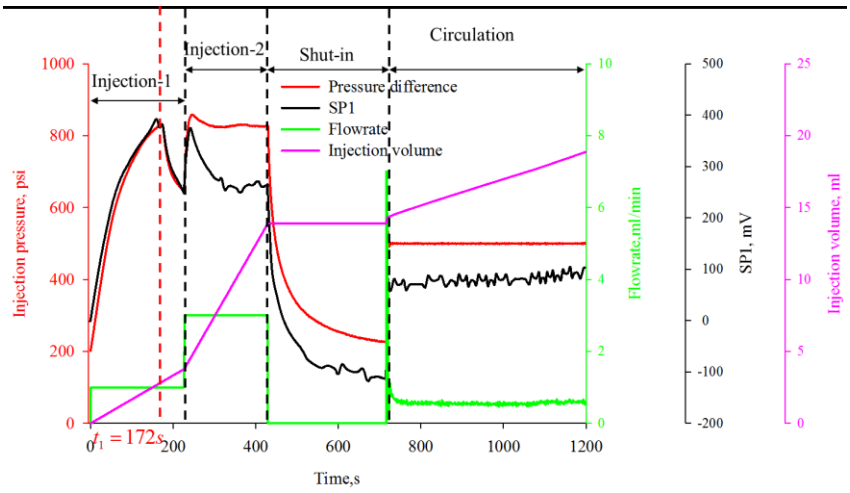

Figure 9: The recording data for Sierra White granite block test (second cycle)

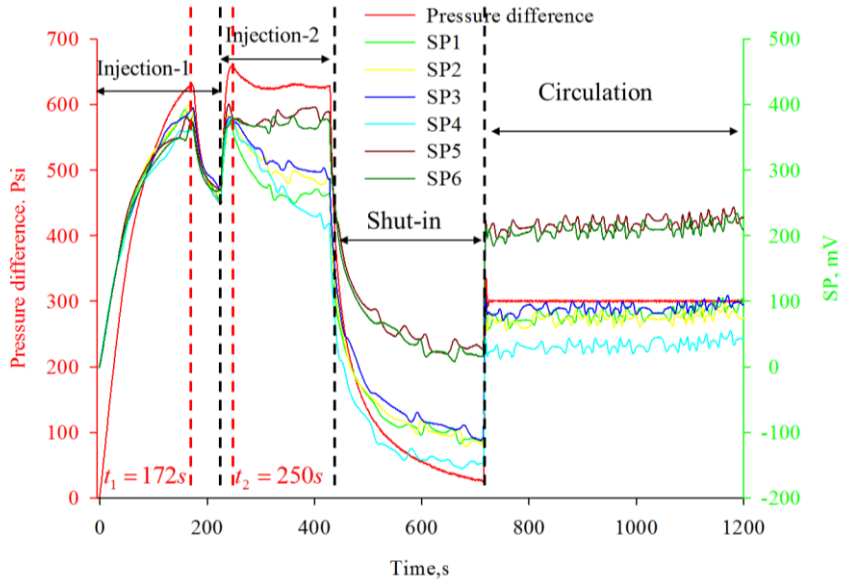

Figure 10: The SP data with pressure drop (second cycle)

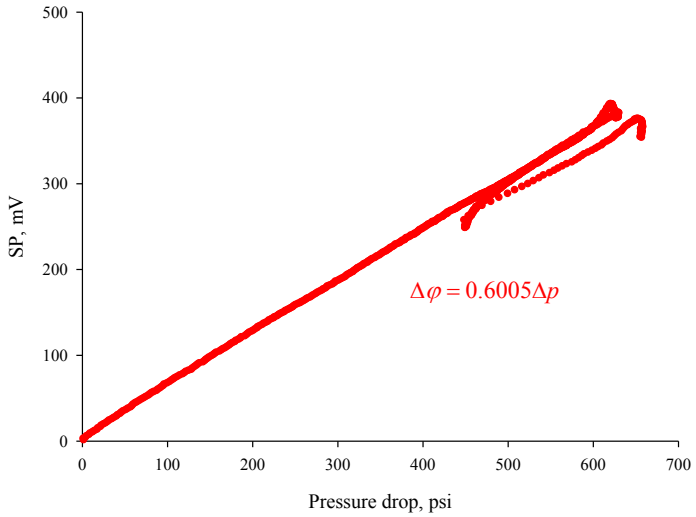

Figure 11: The electrokinetic coupling coefficient for different intervals (second cycle).

3.4 Induced Fracture Geometry and Tracer Analysis

After the test, water containing a red dye was injected into the rock block at low pressure. Water was observed coming from one of the block surfaces on which the SP sensors were located. Figure 12 is an image showing the relative location of the fracture and the SP sensors. The fracture trace on the rock surface is at an angle of about 33 degree from the vertical line and is about 3.5 in long. After cutting the rock along the red dotted line, Figure 13 shows the fracture trace on the cut surfaces (the red curves). According to what can be observed on the surfaces, two fractures initiated at the wellbore. It appears that both segments occurred during the first stage and they merged to form one fracture and propagated to the south surface of the block on which the minimum horizontal stress was applied. As previous pressure and SP transient analysis shows, the final fracture geometry was the result of two stimulation treatments with different in-situ stress conditions.

Theoretically, the induced fracture would be expected to propagate along the direction of maximum horizontal stress such that a vertical and a horizontal fracture would form during the first and the second stages, respectively. This ideal prediction is not observed and is likely caused by rock heterogeneity and low stress contrast particularly during the first fracturing-circulation. Close inspection showed that the fracture followed a white zone within the rock block consisting of the mineral Albite. Figure 14 is a thin section of Sierra White granite. Analyzing the image it is found that dark parts on the images are Quartz and the light parts are Albite. Some broken Quartz crystals are also visible on the images. The fracture may just follow the weak boundary between the Quartz and Albite grains or may cut across the Albite grains. Thin section observations of the fracture zone are currently underway. The propagation of the fracture during the second cycle was influenced by the pre-existing fracture but it changed to a horizontal fracture for a short distance before turning again. Overall, a larger stress contrast appears to be needed to overcome the influence of the rock fabric.

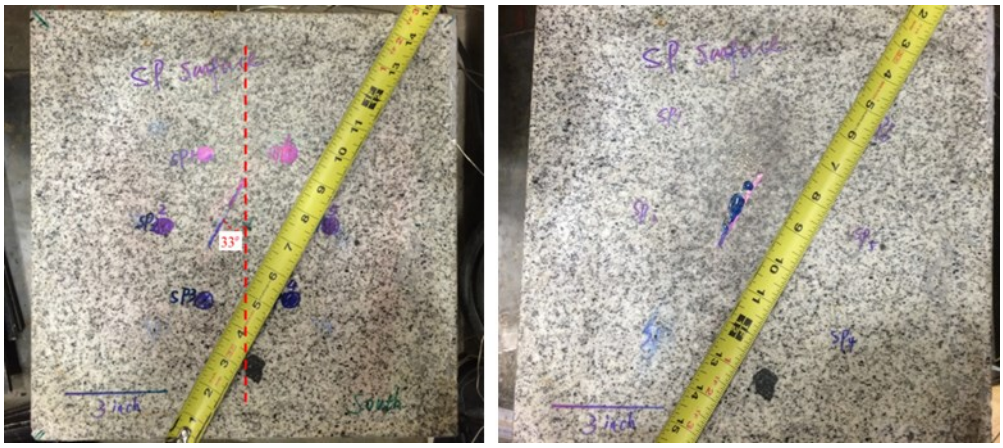

Figure 12: Fracture on the rock surface on the left (indicated by the blue mark at the center). The right image shows water drops flowing out of the fracture.

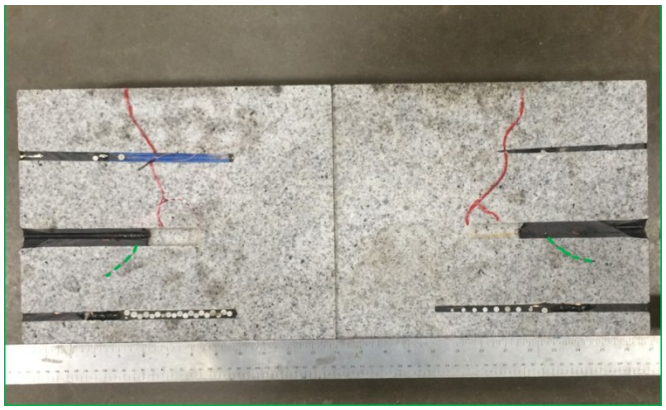

Figure 13: Fracture on the cut surfaces (indicated by the red curves). Green curves show a less visible fracture trace.

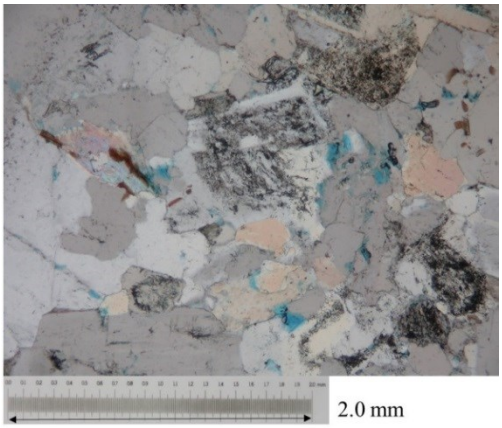

Figure 14: Thin section for Sierra White granite. Blue shows pores and cracks. Quartz, albite, biotite, and muscovite grains are visible (inspection of the cracks in the tested block shows they tend to follow the albite cleavage and/or grain boundaries).

As shown in Figure 3, four production wells were drilled surrounding the injection well. Unfortunately, three of these wells were inadvertently plugged by the epoxy including the one intersected by the induced fracture. So, even with two circulation steps, with the pressure in the open production well maintained at atmospheric pressure, the production rate was very small. After the first fracturing step, about 3.3 ml of production fluid was collected during the first 30 minutes and 1.8 ml during the next 60 minutes. After the second fracturing step, 1.0 ml of fluid was collected during the first 25 minutes. The average flow rates for these time intervals are 0.11 ml/min, 0.03 ml/min and 0.04 ml/min respectively. The abnormal high flow rate observed in the first 30 minutes during the first circulation may result from some air trapped in the relief valve. The chemical analysis shows that the production fluid mainly came from the rock matrix not from the injection well through the fracture, which is reasonable since this production well was not interested by the fracture. The production rate during the test is much lower than the injection rate, which is also commonly observed in full-scale field development.

The permeability of small discs of Sierra White granite was measured and these results show that Sierra White granite has an intrinsic permeability of approximately 10^{-18} m^2. During the circulation stage of the second test cycle, an injection rate of about 0.6 ml/min was achieved at an injection pressure of 500 psi. Using the Cubic Law (Ishibashi and Takuya, 2012), we obtain a much higher permeability of the order of 10^{-11} m^2, presumably because of fracturing effects.

4. ACOUSTIC EMISSIONS

More than 12,000 hits were recorded during the first fracturing stage but the number of recorded events that were located spatially was far smaller. Figure 6 shows about six hundred located AE events. Figure 15 shows the located AE events next to a vertical section through the block showing the traces of fractures. The fracture indicated by the dashed line is not as conspicuous as the other fracture shown. The AE event locations tend to generally correlate with the location of the fractures that were formed during the first fracturing cycle. Actually, the AE events are concentrated in two zones, an upper zone and a lower zone. The lower cloud clearly correlates with the fractures that are visible in the lower part of the wellbore and apparently extended to coalesce during the first injection step. The upper cloud tends to correlate with a less visible (due to some rock removal by the saw) fracture trace shown in Figure 13 (green dashed line). The AE monitoring system was shut off during the second stage of fracturing and so no data is available for comparison. The relatively low quality of the AE waveform in the first stage is responsible for lower than expected number of events, making direct and conclusive correlation with fracture traces difficult. The low quality of the AE signals is likely caused by the fact that the all the AE sensors and their wires are submerged in saline water under pressure. A notched beam fracture toughness test shown in Figure 16 was successfully conducted on a sandstone beam and verified the feasibility of our AE system. The AE-determined fracture geometry is in very good agreement with the real fracture geometry and even indicates the indentation caused by the support bar. Corrective action will be needed to improve signal quality for submerged block tests.

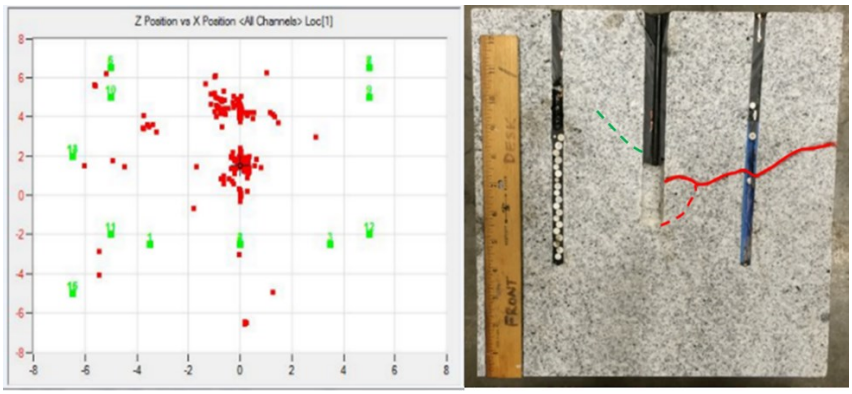

Figure 15: Notched beam fracture toughness test and the AE-determined fracture geometry.

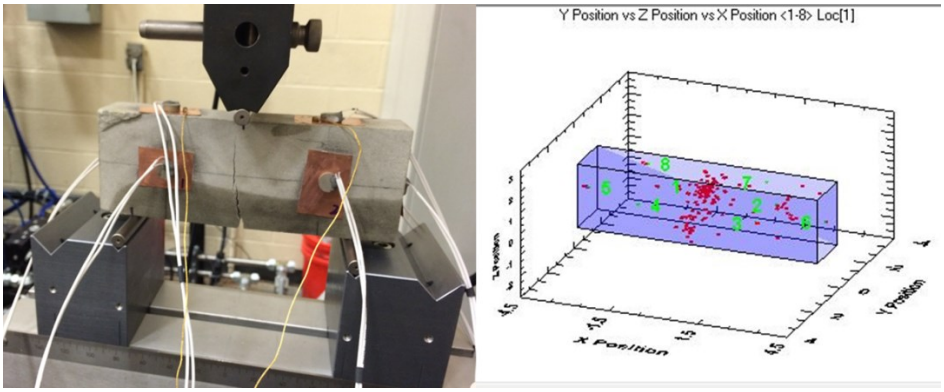

Figure 16: Notched beam fracture toughness test and the AE-determined fracture geometry.

5. CONCLUSION

A new lab-scale polyaxial hydraulic fracturing test system has been developed. It allows EGS fracturing stimulation and fluid circulation to be simulated on laboratory scale. Preliminary tests on a saturated granite block illustrated and verified the functionality of the system. The preliminary tests show an excellent relationship between SP response and the pressure drop during hydraulic fracturing. The block test shown here as well as others not reported illustrate AE activity that generally corresponds to fracture initiation and propagation. Additional sensors and modification of sensor installation should provide better correlation between the AE cloud and the hydraulic fractures. The post-test fracture geometry analysis indicates the complexity of induced fracture geometry under low in-situ stress conditions and the effects of the presence of pre-existing fabric and mineral heterogeneity.

ACKNOWLEDGEMENTS

This project was supported by the U.S. Department of Energy Office of Energy Efficiency and Renewable Energy under Cooperative Agreement DE-EE0006765.0000. This support does not constitute an endorsement by the U.S. Department of Energy of the views expressed in this publication. The authors would like to thank two reviewers for their comments and suggestions that have improved the paper. We also thank Dr. T. Ishido for discussions and suggestions regarding SP measurement.

REFERENCES

Fitterman D V. 1978. Electrokinetic and magnetic anomalies associated with dilatant regions in a layered earth. Journal of Geophysical Research: Solid Earth. 83(B12): 5923-5928.

Hubbert, M.K. and Willis, D.G. 1957. Mechanics of Hydraulic Fracturing. *Transactions of AIME*. 153-166.

Ishido, T., and Pritchett, J. W. 2003. Characterization of fractured reservoirs using continuous self-potential measurements. *In Proc. 28th Workshop on Geothermal Reservoir Engineering*. 158-165

Ishibashi T, Watanabe N, Hirano N, et al. 2012. Experimental and Numerical Evaluation of Channeling Flow in Fractured Type of Geothermal Reservoir. *Thirty-Seventh Workshop on Geothermal Reservoir Engineering*, Stanford University, Stanford, California.

Jouniaux L, and Pozzi J P. 1995. Streaming potential and permeability of saturated sandstones under triaxial stress: Consequences for electrotelluric anomalies prior to earthquakes. *Journal of Geophysical Research: Solid Earth*. 100(B6): 10197-10209.

Moore, J.R., and Glaser, S.D. 2007. Self-potential observations during hydraulic fracturing. *Journal of Geophysical Research: Solid Earth* 112.B2.

Morgan, F. D. 1989. Fundamentals of streaming potentials in geophysics: Laboratory methods. *In Detection of subsurface flow phenomena*. Springer Berlin Heidelberg. 133-144

MIT-Led Report. 2006. The Future of Geothermal Energy, ISBN: 0-615-13438-6.

Pritchett, J. W., and Ishido, T. 2005. Hydrofracture characterization using downhole electrical monitoring. *In Proceedings of World Geothermal Congress*, Turkey.

Yang Y, Zhang L, Lv J, et al. 2012. Experimental study on fracture process of concrete by acoustic emission technology. *Przegląd Elektrotechniczny*. 88(9b): 55-58.